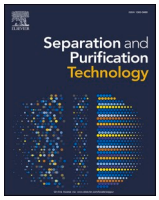
Separation and Purification Technology 380 (2026) 135188



Contents lists available at ScienceDirect

Separation and Purification Technology

journal homepage: www.elsevier.com/locate/seppur





Ultra-high purification efficiency of magnesium via liquid aluminum

An Wang, Si-Ying Lu, Bo-Yu Liu, Rong-Chang Zeng, Zhi-Wei Shan *

State Key Laboratory for Mechanical Behavior of Materials, Xi'an Jiaotong University, Engineering Research Center for Magnesium-based New Materials, Center for Advancing Materials Performance from the Nanoscale (CAMP-Nano), Xi'an 710049, People's Republic of China

ARTICLE INFO

Keywords:
High-purity magnesium
Vacuum distillation
Negative deviation solution
Aluminum melt
Magnesium vapor

ABSTRACT

Magnesium (Mg), prone to impurity-induced degradation even at ppm levels, is traditionally purified through vacuum distillation in industrial settings. However, entrainment of impurities in the Mg vapor reduces separation efficiency, thereby necessitating multiple distillation steps to obtain high-purity (HP) Mg (>99.999 wt%, 5 N). To address this limitation, aluminum (Al) melt was introduced into the vacuum distillation process to absorb impurities from Mg vapor actively. Impurity elements, such as Fe, Ni, Cu, Al, Si, and Ca can be reduced to concentrations below 0.1 ppm. Zn, a challenging impurity to remove through conventional vacuum distillation, can be reduced to 1.78 ppm by increasing the crystallization temperature to 620 °C. With this approach, crude Mg with a purity 99.6 wt% can be directly refined to 99.9997 wt% (5 N7) ultrahigh-purity (UHP) Mg in a single distillation step. This novel approach, by introducing liquid metals into the vacuum distillation process, significantly enhances purification efficiency and increases the feedstock's impurity tolerance.

1. Introduction

The corrosion resistance of magnesium (Mg) and its alloys is highly sensitive to trace impurities such as iron (Fe), nickel (Ni) and copper (Cu), which can accelerate degradation and restrict their application [1–5]. Even at concentrations of just a few parts per million (ppm), these elements can substantially increase the corrosion rates, drastically shortening the in-service life of Mg components [6]. High-purity (HP) Mg is also essential as a reducing agent in titanium sponge production [7]. However, residual aluminum (Al) impurities present in commercial Mg ingots can be transferred into titanium, compromising the purity of the final titanium product [8]. To enhance both the corrosion performance of Mg alloys and the quality of derived metals such as titanium, it is imperative to develop methods that effectively lower impurity content in Mg feedstock.

Vacuum distillation is a common method for producing HP Mg by leveraging the difference in evaporation rates between Mg and non-volatile [9] impurities, such as Fe, Ni, and Cu. Under vacuum, Mg readily evaporates, while these impurities remain in the residue. Since evaporation rates scale approximately with saturated vapor pressure [10], the process is theoretically effective. For example, at 750 °C, the vapor pressure of silicon (Si) is roughly 3×10^{-13} of that of Mg, suggesting that Si concentrations could be reduced to the order of 1×10^{-13} wt% ($\sim 10^{-7}$ ppm) following distillation. However, in practice, impurity removal falls far short of this theoretical value. A single vacuum distillation at 750 °C reduces Si content from 37 ppm to only 3.5 ppm [11], corresponding to a separation efficiency of 9.5 % (the ratio of impurity contents after and before distillation, where a lower value indicates better separation), orders of magnitude above the expected value. This discrepancy is observed not only for Si but across a broad range of involatile impurities. As a result, multiple distillation cycles are required to achieve high purity, driving up both energy consumption and cost.

The limited effectiveness of vacuum distillation largely stems from the unintended transfer of impurity elements in solid or liquid form, rather than through vaporization, and, as a result, end up in the final Mg products. Boiling occurs when a liquid's saturated vapor pressure exceeds the surrounding pressure, initiating widespread vapor nucleation and escape from the liquid phase. Once vapor passes through the liquid surface, it disrupts the liquid films, producing microdroplets through film breakup [12,13]. These microdroplets, with high drag coefficients [14], are easily entrained by the vapor flow. In typical Mg vacuum distillation systems, operating pressures are usually below 10 Pa [15–17], far lower the Mg's saturated vapor pressure of 350 Pa at its melting point (650 °C). It means that Mg will boil once the evaporation temperature is higher than the melting point, making droplet formation inevitable. Thus, microdroplets, carrying the similar composition as unrefined feed, are transported with the vapor and contaminate the condensed Mg crystal, reintroducing impurities. Additionally, solid

* Corresponding author.
E-mail address: zwshan@mail.xjtu.edu.cn (Z.-W. Shan).

https://doi.org/10.1016/j.seppur.2025.135188
Received 3 June 2025; Received in revised form 8 September 2025; Accepted 13 September 2025
Available online 15 September 2025
1383-5866/© 2025 Elsevier B.V. All rights are reserved, including those for text and data mining, AI training, and similar technologies.

particulates, such as oxides, present at the evaporation interface can also be easily carried by Mg vapor into the final crystal [18].

Another major limitation of conventional vacuum distillation is the absence of active mechanisms to prevent impurities from reaching the final product. When Mg vapor travels toward the condensation zone, any entrained impurities, whether in liquid, solid, or droplet form, will directly be incorporated into the product unless actively intercepted. To address this, several approaches have been proposed that use porous materials to filter impurities during vapor transport. For example, Liang [18] demonstrated the use of millimeter-scale porous media to capture impurities from Mg vapor. Our previous works [19–21] explored the use of materials such as porous Fe, Ni, and Si to actively trap and remove impurities.

The effectiveness of porous filters relies heavily on their chemical reactivity with impurities. When impurities come into contact with the filter surface, they react to form compounds that coat the material. However, due to the low diffusion rate in solid materials [22,23], these reaction products accumulate on the surface rather than diffusing inward, leading to rapid passivation and reduced reactivity over time. This surface passivation effect limits the long-term efficiency of solid filters. In addition to chemical trapping, porous filter materials can physically intercept impurity particles, with effectiveness depending on the filter's pore size. Nevertheless, filters with micrometer-scale pores, which could capture smaller particles, generate excessive flow resistance, making them impractical. Conversely, millimeter-scale porous foam, such as those used in the Liang's work [18], allow better flow but cannot effectively capture micrometer-scale particles. These challenges underscore the need for a new filtration system that offers both high impurity removal capacity and extended in-service life.

To overcome the limitations of conventional filtration, here we introduce a novel melt-assisted purification method. In this approach, Al melt is placed within the vapor flow channel of a vacuum distillation apparatus, between the evaporation and crystallization sections. As Mg vapor passes through, the Al melt acts as a chemical trap, absorbing vapor-state impurities by establishing phase equilibrium between the Al melt and the impurity vapors. For more volatile impurities, such as zinc (Zn), they can be removed by increasing the crystallization temperature. Using this novel approach, industrial crude Mg can be directly refined into ultrahigh-purity (UHP) Mg with a purity of 99.9997 wt% (5 N7) in a single distillation step, eliminating the need for multiple distillation cycles.

2. Purification principle

The purification of Mg relies on inducing relative motion between Mg atoms and impurities species. During evaporation, Mg atoms transition into the vapor phase, while most impurity remain in the crucible. However, separation does not cease there. The transport of vapor and the subsequent condensation also involve relative motion between atoms, which may further contribute to impurity removal. Enhancing purification efficiency, therefore, requires either introducing new forms of relative atomic motion, or improving those already present in the system. This work pursues both strategies: introducing a reactive Al melt to selectively capture impurities from the Mg vapor, and optimizing the crystallization process by increasing crystallization temperature to enhance the purity of the condensed Mg.

2.1. Selection criteria for reactive melt elements

To avoid introducing new contaminants during purification, the added filter material must not exceed the impurity limits already defined for commercial Mg, such as those specified by China's National Standard for Primary Mg Ingots (GB/T 3499–2023). Additionally, to prevent loss through evaporation, the introduced filter material must exhibit a significantly lower vapor pressure than Mg. We set a vapor pressure ratio threshold of 10^{-6} (corresponding to 1 ppm impurity level to Mg) to define acceptable candidates. Elements meeting this requirement include Al, Sn, Cu, Fe, Si, Ni, and Ti, as shown in Fig. 1(a).

The selected element must also effectively absorb impurity vapor without becoming rapidly passivated. Materials with high atomic diffusivity are preferred, as they allow continuous uptake of impurities by preventing surface blockage. Since diffusion rates in liquids are generally several orders of magnitude higher than that in solids, here we focus on elements that remain liquid at or slightly above Mg's melting point (650 °C). This narrows the viable options to Al and Sn. Moreover, the much higher viscosity of liquid metals compared with Mg vapor [24,25] results in stronger drag forces on impurity particles, in accordance with Stokes' Law [14]. This enhanced drag can reduce particle mobility, leading to the effective entrapment and separation of impurities from the Mg vapor.

Economic considerations further favor the use of Al. At 20,590 yuan (RMB) per ton, Al is nearly twelve times less expensive than Sn (248,150 yuan per ton) [26], making it a cost-effective choice for large-scale implementation.

2.2. Impurity absorption ability of Al melt

The absorption capacity of the Al melt for impurities can be evaluated from the equilibrium impurity concentration in Mg vapor. This concentration corresponds to the theoretical minimum impurity level after purification, which can be obtained from the partial pressures of the vapor components [27]. Since the partial pressure of most impurities is relatively low, it is reasonable to approximate the total gas-phase pressure with the saturation vapor pressure of Mg at the evaporation temperature. The partial pressure of impurity in Mg vapor is equal to the equilibrium partial pressure of impurity in the Al melt. The resulting mass concentrations of each impurity in the vapor can be estimated as follows:

$$y_i = \frac{P_i M_i}{P^o_{\mathrm{Mg}} M_{\mathrm{Mg}}} = \frac{x_i \gamma_i P^o_i M_i}{P^o_{\mathrm{Mg}} M_{\mathrm{Mg}}} \# \tag{1}$$

Where y_i, P, and M denote the impurity concentration, vapor pressure, and relative atomic mass, respectively. The subscripts i and Mg refer to the impurity and Mg, respectively. The superscript o denotes the equilibrium vapor pressure. x_i is the mole fraction of the impurity in the melt, and γ_i is its activity coefficient.

A solution with negative deviation from Raoult's law is expected when impurities interact strongly with Al. In such a solution, the activity coefficient of the solute is below 1, indicating strong interactions between the components. According to Eq. (1), the impurity's activity coefficient, along with its concentration and saturated vapor pressure, collectively governs its content in Mg vapor. A lower activity coefficient reduces the tendency of impurities to enter the vapor phase, thereby decreasing their vapor concentration and providing an effective purification mechanism. Thermodynamic calculations (Fig. B1, Appendix B) show that Al forms negative-deviation binary solutions with key impurities such as Fe, Mn, Ni, Ti, Cu, Si, and Ca, whereas the Al—Pb and Al—Zn systems exhibit positive deviation and near-ideal behavior, respectively.

As shown in Fig. 1(b), the impurity equilibrium concentration in the Mg vapor increases with its concentration in the Al melt. The right end of each curve represents the solubility limit in the binary Al-impurity melt, with 50 % indicating completely miscible. Most impurities, such as Si, Mn, Cu, and Fe, can be removed to below 1 ppm, even when their concentration in the Al melt reaches the solubility limit. Elements like calcium (Ca), particularly in oxide form, are also easily captured by the Al melt. In contrast, Zn and Pb remain difficult to remove due to their high volatility and weak interaction with Al melt.

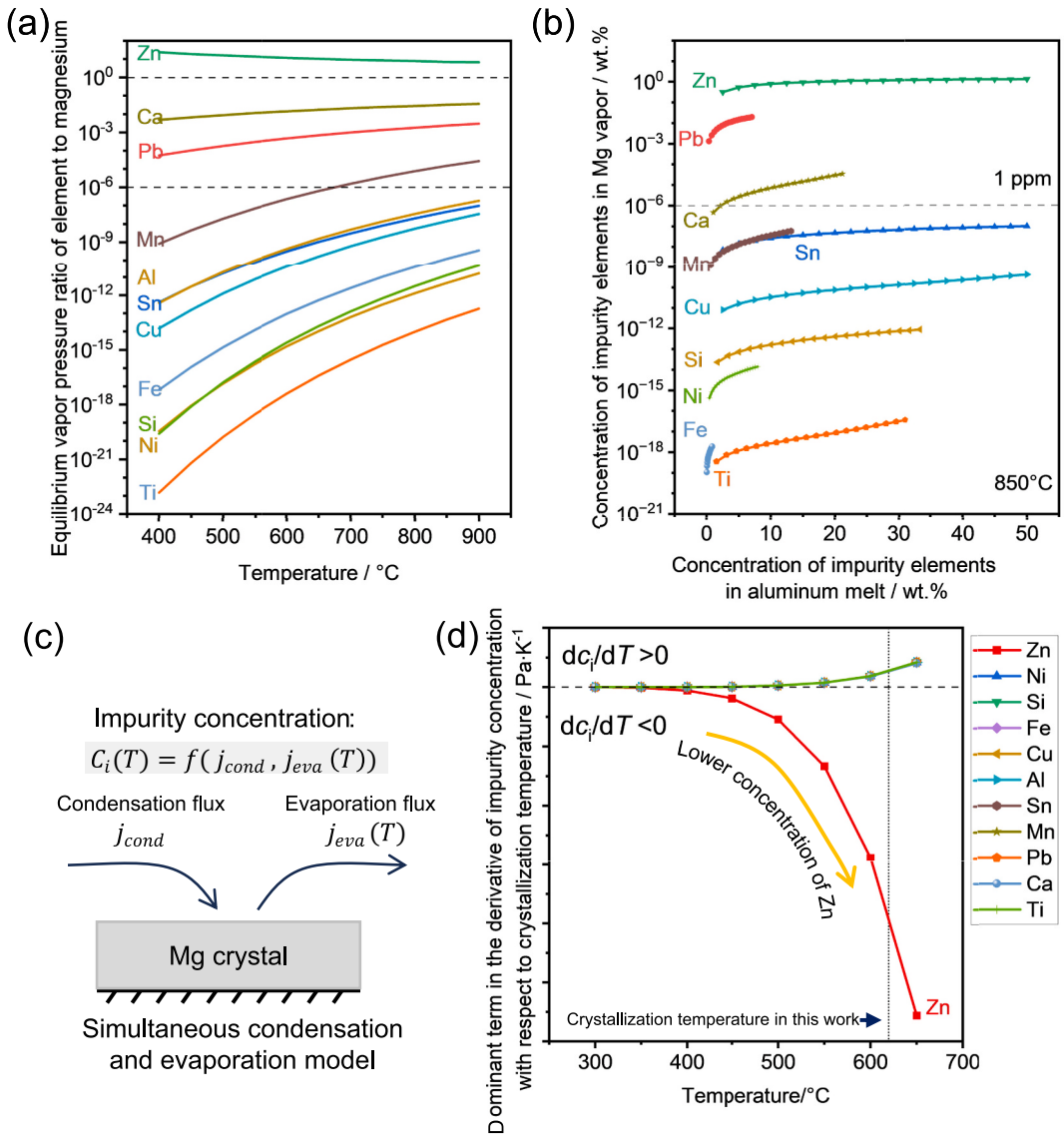


Fig. 1. Purification of Mg vapor through active impurity absorption and increased crystallization temperature. (a) The ratio of the saturated vapor pressure of metal elements to that of Mg. Only Al, Sn, Cu, Fe, Si, Ni, and Ti meet the requirement of not contaminating Mg vapor, given an upper limit of 10^{-6}. Considering the melting point and cost factors, Al is ultimately chosen. (b) The equilibrium concentrations of impurities in Mg vapor after purification by the Al melt. Within the solubility limit of the Al melt, impurities such as Mn, Sn, Cu, have an equilibrium concentration of less than 1 ppm in the Mg vapor. Calcium, often existing in the form of an oxide, readily adheres to aluminum melts and can be removed from Mg vapor. Zinc and Pb, however, are not easily removed by the Al melt. (c) The condensation model for the vapor-solid phase transition. The net condensation of vapor is determined by both the incoming vapor flux and the evaporation flux of the condensate surface. (d) The derivative of impurity concentration with respect to temperature during the condensation process. Only the derivative of Zn impurity concentration is negative, suggesting that Zn content can be reduced by increasing the crystallization temperature.

2.3. Enhancing Zn removal via crystallization temperature control

The vapor-to-solid condensation process offers another opportunity for impurity separation. During crystallization, the net deposition rate is governed by the balance between incoming vapor condensation and the surface evaporation, as schematically shown in Fig. 1(c). At equilibrium, impurity incorporation into the solid depends solely on temperature. The temperature dependence of impurity concentrations is quantified by their derivatives, as shown in Fig. 1(d) and derived in detail in Appendix A. Among the impurities studied, only the Zn exhibit a negative derivative, indicating its concentration in the crystal decreases as the crystallization temperature increases. Moreover, the derivative becomes more negative with higher temperatures, implying an increasingly efficient removal of Zn with each incremental rise in temperature. To avoid melting the deposited MG while maximizing Zn exclusion, crystallization was carried out just below Mg's melting point.

Briefly, our purification strategy combines two key aspects: a molten Al filter introduced between the evaporation and crystallization zones to actively absorb impurities, and an elevated crystallization temperature to selectively reduce Zn incorporation.

3. Experimental setup

A vertical tube furnace equipped with graphite tubes was used to serve as the container for Mg vapor phase change and flow. The core structure consisted of nine threaded graphite tubes connected end-to-end, each with an inner diameter of 40 mm, outer diameter of 60 mm, and length of 100 mm, as shown in Fig. 2(b). A graphite plate with a central opening served as the crystallizer, positioned to collect condensed Mg vapor.

Two concentric tubes were placed between the evaporation and crystallization zones, which housed the Al melt. This design ensured that

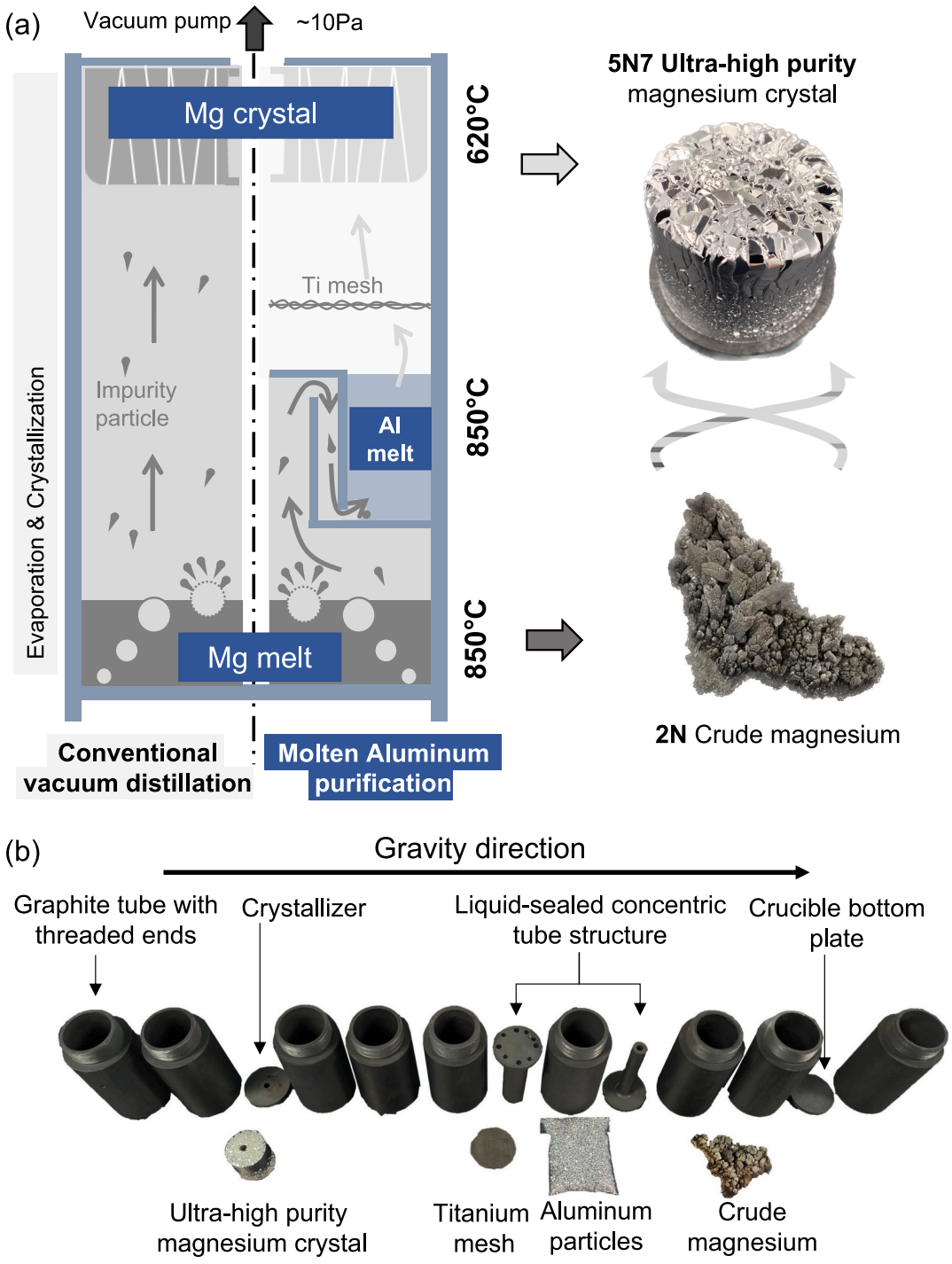


Fig. 2. Schematic diagram of the experimental setup. (a) Schematic illustration of Mg vapor movement. In traditional vacuum distillation, the vapor carries a large number of impurities. After introducing the Al melt, it can absorb the impurities carried by the Mg vapor. (b) Experimental setup diagram. Nine graphite tubes were connected to form a container for phase transition and vapor flow of Mg. The graphite bottom plate and crystallizer, combined with the graphite tubes, constituted the evaporation and condensation zones, respectively.

Mg vapor flowed through the Al melt, while the Al melt did not flow back into the evaporation zone due to gravity. A titanium (Ti) mesh, chosen for its low saturated vapor pressure, was placed at the outlet of the concentric structure to capture impurities carried by the Mg vapor and to asses purification efficiency. The morphology and composition of the Ti mesh were analyzed using scanning electron microscopy (SEM) and energy dispersive spectroscopy (EDS). The overall Mg vapor flow path is schematically shown in Fig. 2(a).

To compare the impurity removal efficiencies with and without the presence of Al melt, three types of evaporation experiments with different graphite tube structures were designed. The first, a baseline setup, involved direct evaporation with only graphite tubes and a crystallizer. The second, termed evaporation-CC, incorporated two concentric tubes into the baseline structure but did not include Al melt. The third setup, referred to as the molten aluminum purification (MAP), was identical to the second evaporation-CC setup but included molten Al in the concentric tubes. By comparing the results from the evaporation-CC and MAP experiments, the effect of the Al melt could be isolated from

that of the concentric tubes, allowing a direct assessment of its impurity removal capability.

The tube furnace was divided into three heating zones: evaporation, Al melt, and condensation. These zones were set to 850 °C, 850 °C, and 620 °C, respectively, with a holding time of 2 h and a heating rate of 10 °C/min. The evaporation zone was maintained at 200 °C above Mg's melting point (650 °C) to enhance the Mg evaporation rate. The crystallization zone was held at 620 °C, as mentioned previously, to suppress Zn incorporation into the crystallized Mg.

Al particles of 4 N-purity were placed inside the concentric tubes, which, upon melting, formed a liquid seal structure. Mg vapor passed through this structure and was purified by the Al melt. A titanium mesh was placed at the outlet of the concentric tubes to intercept impurities carried by the Mg vapor and to serve as an indicator of the impurity content in the vapor. Due to its high melting point and a lack of a eutectic reaction with Mg [28], Ti mesh maintains its structural integrity and resists corrosion at experimental temperatures. Its high boiling point further ensures that it will not evaporate and contaminate the Mg vapor.

To allow Mg vapor to pass through the Al melt, the static pressure of the Al melt bottom must not exceed the saturated vapor pressure of Mg at the evaporation temperature. The relationship between static pressure and evaporation temperature is as follows:

$$h = \frac{aP^{o}_{Mg}(T_{eva})}{\rho_{Al} g}\# \quad (2)$$

Where h is the height of the Al melt, ρ_{Al} is its density, g and T_{eva} designate the acceleration due to gravity and the evaporation temperature, respectively. The hydrostatic pressure of the liquid-seal structure establishes the maximum back-pressure that can resist the vapor flow [29]. This back-pressure defines the threshold above which Mg vapor cannot escape through the liquid seal, thereby determining the effective limit of inhibition on Mg evaporation. In this work, the coefficient a, defined as the ratio of the hydrostatic pressure to the saturated Mg vapor pressure, must remain below 1. To allow Mg vapor to successfully overcome the melt and pass through the seal, this coefficient was set to 23.84 %. Before heating, the tube furnace was evacuated to a pressure below 10 Pa.

The raw material for evaporation was crude Mg, the purity of which is listed in Table 1. The impurity contents in the above materials were measured using ICP-MS (ICP-MS 7850, Agilent) or GD-MS (Element GD Plus, Thermo Fisher). The GD-MS detection range has 76 elements, comprising 64 metallic elements. After excluding Mg, 63 metallic elements remain. The purity of Mg was calculated by subtracting the contents of 63 metal impurity elements from 1.

Thermodynamic calculations were performed using the equilibrium module of the FACTSAGE software. The databases used were the PS and LITE libraries.

4. Results and discussion

The Ti mesh serves as indicator of impurity levels in the Mg vapor by capturing contaminations as the vapor passes through. The morphology of the Ti mesh after the experiment is shown in Fig. 3. In the direct evaporation experiment using crude Mg, the mesh surface (Fig. 3(a-c), Fig. C1(a-d)) was heavily coated with impurities—including Al, Si, Ca, Cl, Fe, and O—indicating significant contamination. If these impurities were directly transferred into the condensed Mg, they would significantly compromise its purity. As shown in Fig. 3(a-c) and Fig. C1(a-d), impurity elements like Si, Fe, and Ca co-existed with Mg and O, that suggests these impurities coexisted with MgO particles may be in non-vapor state carried by the Mg vapor. Given that MgO is thermodynamically stable and in a solid state at the experimental temperature, it is unlikely for impurity vapors to be trapped within MgO particles in such a high-temperature environment. Furthermore, the uniform distribution of Al, Si, and Ca impurities on the titanium mesh (Fig. C1(e-f)) provides strong evidence that the impurities also exist in a vapor phase. Due to the effect of entropy, vapor-phase impurities would thermally diffuse and distribute uniformly within the Mg vapor, resulting in a homogeneous deposition on the Ti mesh upon contact. These solid particles and impurity vapors are the crucial sources of contamination for Mg vapor during vacuum distillation.

In the evaporation-cc experiments, as shown Fig. 3(d-f), fewer impurities were observed, though dark particulate deposits were still present. The concentric tubes can hinder the Mg flow process and decrease the mass flux of Mg vapor, that will decrease the carrying ability of Mg vapor for impurity particles and then to some content decrease the number of impurity particles in Mg vapor. As shown in Fig. 3(d-f) and Fig. C2, EDS confirmed that the impurities on the Ti mesh remained consistent with those in the direct evaporation experiment. Based on the material intercepted by the Ti mesh, the concentric tubes can partially reduce the impurity content in the Mg vapor.

The Ti mesh from the MAP experiment (Fig. 3(g-i)) appeared largely clean, with only a few residual MgO particles. This suggests that MAP can effectively remove impurity particles entrained in Mg vapor. EDS detected no Ca, and Fe impurities on the mesh surface, confirming that the Al melt effectively captured the impurity vapors in the Mg vapor. When Mg vapor flows over molten Al, it may entrain small droplets of the Al melt, whereas gravity tends to pull these droplets back into the liquid Al. The Ti mesh serves as an indicator of possible Al droplets, since Ti reacts with Al and retains it on its surface [30]. In our experiments, under the given evaporation temperature and Al melt height, no traces of Al were detected on the Ti mesh. This result indicates that significant Al contamination did not occur.

The compositions of the crude and purified Mg samples are shown in Fig. 4(a). The starting material was crude Mg obtained via silicothermic method, which contains high levels of Si, Fe, and Ca. In the direct evaporation experiment, the impurity contents of Si, Ca, Pb, and Zn in the crystallized Mg remained above 1 ppm, while the impurity levels of Al and Fe were 0.29 ppm and 0.28 ppm, respectively. The types of Ca and Fe impurities are consistent with those of the impurity elements accumulated on the Ti mesh. After the use of the concentric tubes, the impurity contents of Al, Si, Ca, and other elements in the crystallized Mg significantly decreased. However, the Fe impurity content unexpectedly increased to 2.8 ppm, which can be attributed to Fe-rich impurity particles—similar to those shown in Fig. 3(f), but smaller in size—being transferred into the crystallized Mg. It should be noted that such impurity transport is an uncontrollable contamination process and should be avoided whenever possible. The purity of the crystallized Mg obtained from direct evaporation is 4 N8, whereas the purity of the

Table 1
Impurity contents (ppm) of raw materials and purity (weight percent) of crystalline Mg.

	Impurity contents, ppm											wt%
Element	Al	Si	Ca	Ti	Mn	Fe	Ni	Cu	Zn	Sn	Pb	Mg
Crude Mg	29.42	962.00	753.45	0.22	5.65	2442.9	0.42	0.25	11.80	0.11	5.42	2 N6
Direct evaporation	0.29	1.0	6.9	0.07	0.1	0.28	0.04	<0.05	3.7	0.06	2.3	4 N8
Evaporation-cc	0.05	0.24	2.0	0.02	0.13	2.8	0.05	<0.05	5.1	0.07	1.1	4 N5
MAP-1	0.027	0.088	0.1	<0.005	0.13	0.02	<0.005	0.065	1.78	<0.05	0.17	5 N7
MAP-2	<0.01	<0.01	0.02	<0.005	0.16	<0.005	<0.01	<0.05	3.2	<0.01	1.6	5 N5

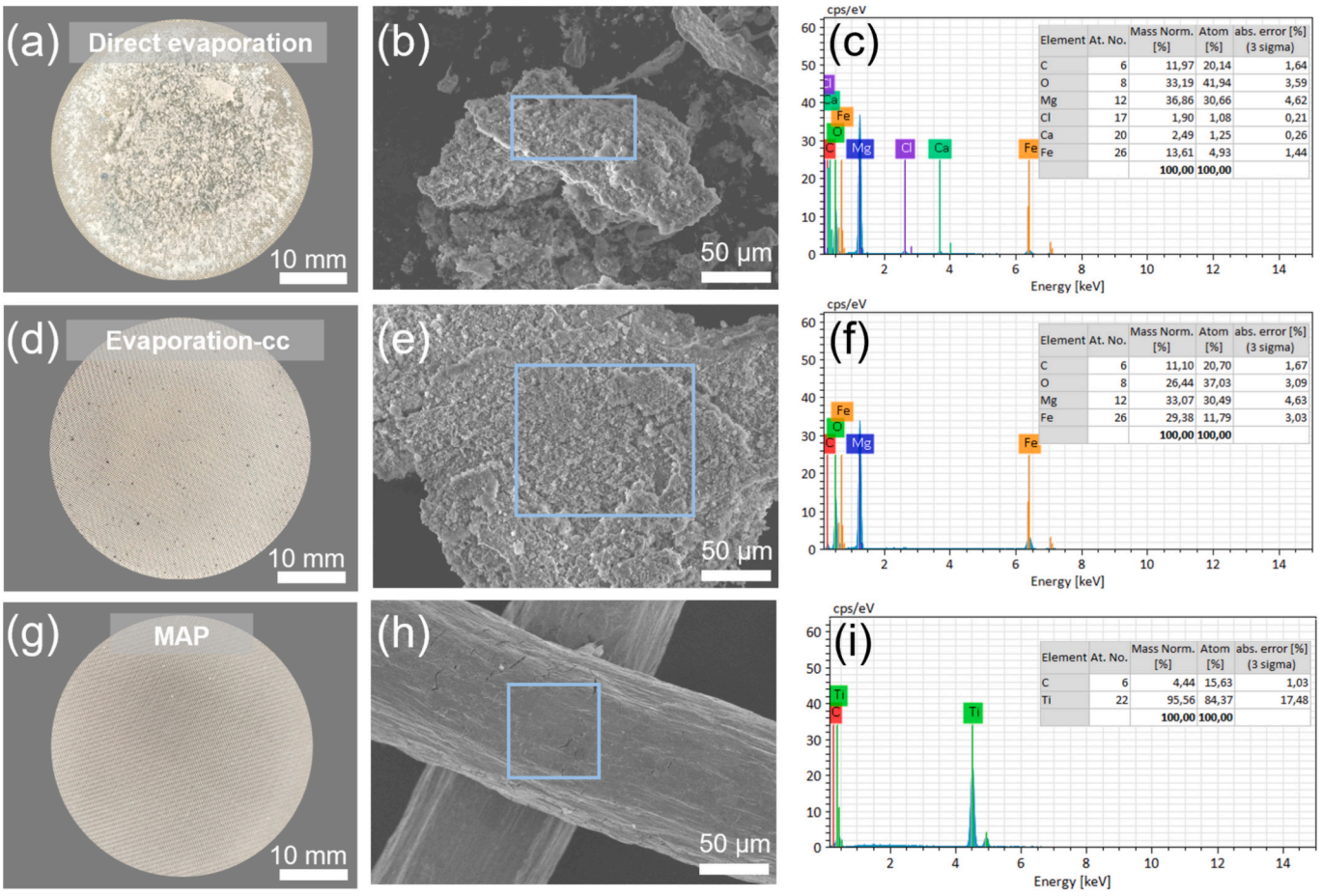


Fig. 3. Aluminum melt effectively removes impurities carried by Mg vapor compared to direct evaporation and direct evaporation with concentric tubes. (a-c) reveal that after the direct evaporation of crude Mg, a significant accumulation of impurities, including Ca, Cl, Fe, and O, was observed on the surface of the Ti mesh. (d-f) show the surface morphology of the titanium mesh following the evaporation experiment with the introduction of concentric tubes positioned in front of the mesh. The presence of the concentric tubes did not alter the types of impurities captured by the Ti mesh but effectively reduced the quantity of impurities collected. (g-i) present the surface morphology of the Ti mesh after the MAP experiment. The Al melt successfully absorbed the impurities carried by the Mg vapor, resulting in an almost impurity-free Ti mesh post-experiment.

crystallized Mg from the concentric tubes experiment is 4 N5. The lower purity in the latter case is attributed to an elevated Na content of 25 ppm. It is worth to clarify that while we refer to our setup as "direct" distillation, it differs from traditional direct distillation by including a Ti mesh in the vapor flow path. Although the Ti mesh was intended primarily for assessing impurity levels in the Mg vapor, it inadvertently captured some impurities, resulting in a increasement of purity. Compared to the direct distillation of crude Mg in the literature [31], the purity of the crystallized Mg in this experiment increased from 3 N8 to 4 N8. Nevertheless, neither direct evaporation and evaporation-CC was sufficient to elevate the purity of the crystallized Mg to above 5 N.

The purity of the crystallized Mg in the MAP experiment reached 5 N7 and 5 N5, representing a substantial improvement over previous methods. The concentrations of impurities such as Al, Si, Ca, Fe, and Ni in the crystallized Mg significantly decreased, indicating that the Al melt effectively absorbed these impurities. This conclusion is further supported by the clean surface of the Ti mesh after the experiment, which indicates minimal residual impurities in the Mg vapor. It's worth noting that Al was still detected in the high-purity Mg. It's currently difficult to determine the source of this trace amount of Al—whether it's from the raw materials or the Al melt—even though the content is already below 0.1 ppm.

However, the differences in the Pb impurity concentrations are small between the HP Mg from the MAP experiments and that from the direct evaporation experiments. Because the Al—Pb and Al—Zn systems do not exhibit the strong negative deviations from Raoult's law needed to suppress solute activity, even trace dissolution of Zn or Pb in liquid Al corresponds to high activities and thus high equilibrium partial pressures. Further uptake of Zn or Pb by the Al melt is therefore not thermodynamically favored. Consequently, passing Mg vapor through an Al melt does not appreciably reduce the Zn and Pb partial pressures in the vapor, leading to low removal efficiency for these elements. Although the Al melt has poor removal efficiency for Pb and Zn, as mentioned in the purification principle, the high crystallization temperature employed in all experiments still led to a reduction in Zn concentration across the samples.

In the experimental study of HP Mg preparation, evaporation temperatures typically range from 400 to 900 °C. From a thermodynamic perspective, the higher the evaporation temperature, the greater the equilibrium concentration of impurities in the vapor phase, which leads to more impurities being incorporated into the HP Mg. Although this study employed a relatively high evaporation temperature of 850 °C, the experimental results show that the impurity removal efficiency is generally superior to that of previous experiments (which is calculated by MAP-1), as shown in Fig. 4(b). This significant advantage can be attributed to the introduction of Al melt, which effectively enhanced the impurity removal process.

In summary, this study provides new insights into the preparation of HP Mg. It also highlights the potential of Al melt for improving impurity removal efficiency. The method shows high tolerance to high impurity

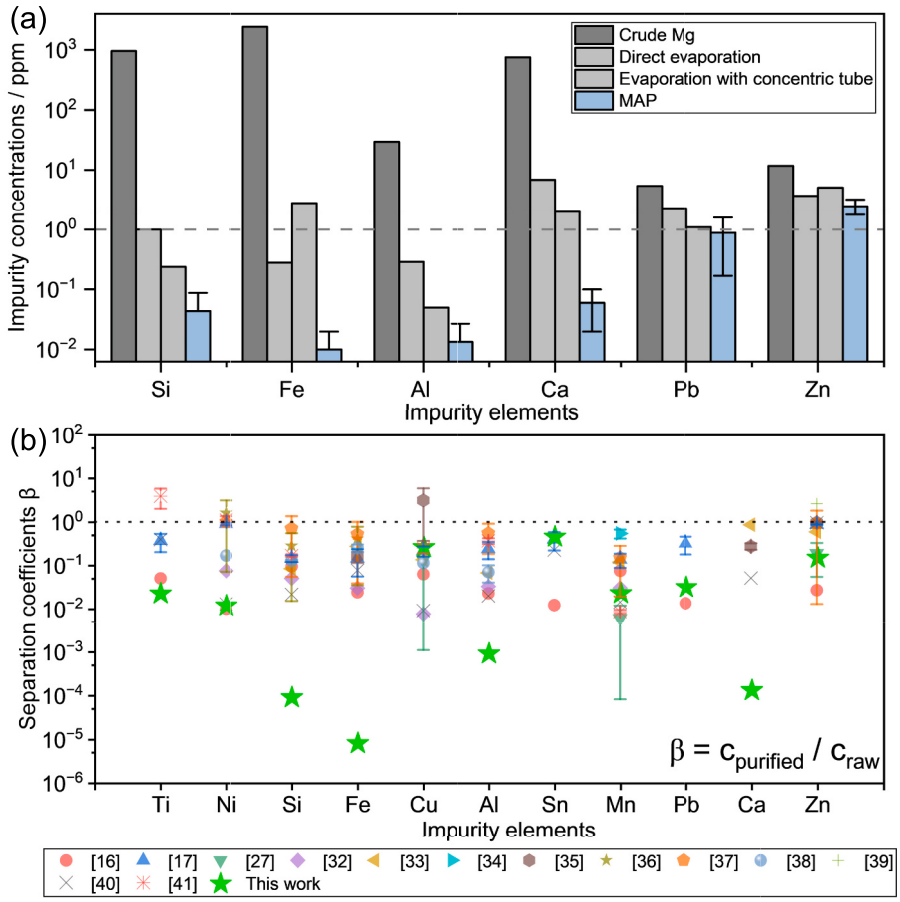


Fig. 4. Impurity contents in crystallized Mg and separation coefficients from the MAP experiment compared to previous studies. (a) The impurity contents in crude Mg and HP Mg. Due to severe contamination, the impurity concentrations in crude Mg, such as Si, Fe and Zn, range from 10 ppm to 2000 ppm. After the direct evaporation and the evaporation experiment with the concentric tubes, the concentrations of impurities such as Si, Fe, Al, and Ca decreased significantly. After purification with the Al melt, the concentrations of all non-volatile impurities in the condensed product were even below their detection limits. Although the reduction in impurities such as Pb was insignificant, the zinc concentration still decreased from 11.8 ppm to 1.78 ppm. (b) Comparison of separation coefficients. A lower separation coefficient indicates better impurity removal efficiency. The purification efficiency for most elements in this study is superior to the results from previous reports [16,17,27,32–41]. The relatively high separation coefficients for Sn and Cu are due to their initially low concentrations.

concentrations in raw materials. Therefore, it can also be used for recycling Mg alloys. However, our findings also reveal limitations in the Al melt's ability to remove Zn and Pb impurities. Therefore, future research will focus on developing alternative strategies for effectively removing these elements, particularly Pb, from Mg vapor.

5. Conclusion

This study introduces the use of Al melt in the vacuum distillation process to effectively remove excessive impurities from Mg vapor, enabling the direct refinement of crude Mg with a purity below 99.9 wt % into ultrahigh-purity Mg with a purity of 5 N7 in a single step.

1) High-boiling-point liquid metals, such as molten aluminum, can be introduced into the vacuum distillation process of crude Mg without causing significant contamination. When the Mg vapor passes through the aluminum melt, the impurities present in the vapor were effectively absorbed by the melt. Non-volatile impurities carried by the Mg vapor were reduced to concentrations below 1 ppm after the purification.
2) A crystallization model based on a layer-by-layer stacking process suggests that among the main impurity elements in crystalline Mg, only Zn—an impurity difficult to absorb by the Al melt—can be markedly reduced, reaching 1.7 ppm when the crystallization temperature is set to 620 °C.
3) Compared to traditional vacuum distillation methods, this novel approach achieves a two-order-of-magnitude reduction in impurity contents within the distilled product.

Notably, this method holds significant potential for enhancing the purification efficiency of other metals in vacuum distillation processes based on the principle of actively absorbing impurities from metal vapor.

CRediT authorship contribution statement

An Wang: Writing – review & editing, Writing – original draft, Validation, Methodology, Investigation, Conceptualization. **Si-Ying Lu:** Methodology, Investigation. **Bo-Yu Liu:** Writing – review & editing. **Rong-Chang Zeng:** Writing – review & editing. **Zhi-Wei Shan:** Writing – review & editing, Project administration, Funding acquisition.

Declaration of competing interest

The authors declare no conflict of interest.

Acknowledgments

Z. W. Shan and his team gratefully acknowledge the support from the National Natural Science Foundation of China (No. 52031011, No. U24A2021 and 52371121), the Science and Technology Departments of Shaanxi Province, China (No. 2023GXLH-029), and the Science and Technology Bureau of Yulin, Shaanxi, China (No. 2023-CXY-199). We acknowledge Bo. Yang, Rui. Zheng, Xiao-Hua. Cheng, Lu-Yao. Mao, Peng-Yong. Wang, Chao-Wei. Guo (Xi'an Jiaotong University) for assistance in this work. We acknowledge Yong-Liang Yang (Fugu TaiDa Coal Chemical Co. LTD) for providing the raw material.

Appendix A. Model for crystallization process

Vapor undergoes a phase transition to either the liquid or solid state when its chemical potential exceeds that of the liquid or solid phase. Considering Mg vapor in a tubular furnace, Mg vapor flows from a higher temperature zone to the crystallization zone. Condensation initiates at the wall, where heat exchange with the vapor increases the chemical potential difference between the Mg vapor and its liquid or solid state. This condensation process relies on the heterogeneous nucleation of Mg vapor, involving collisions between Mg atoms and the furnace wall. For this nonequilibrium process, both the chemical potential difference and kinetic factors, such as collision frequency and collision efficiency, determine the condensation process. The cylinder tube wall exhibits a lower collision efficiency than the baffle vertical to the flow direction, attributed to the difference in the flow resistance caused by these structures. The lower the collision efficiency, the less the condensate. Consequently, the Mg condensate on the cylinder tube wall is negligible and can be disregarded. The vertical baffle, initially meeting the condensation condition of Mg vapor, is considered a primary condensation zone with its temperature referred to as the primary crystallization temperature

The evaporation of the condensate occurs concurrently with the condensation of Mg vapor. The net condensation flux is the difference between the evaporation and condensation fluxes. Here, we assume that the state of the incoming Mg vapor flow remains constant. Considering the crystallization process as a layered stacking model, the deposition product from the previous moment determines the subsequent evaporation process, and the constant-pressure Mg vapor with a fixed impurity concentration colliding with the interface governs the condensation process. Thus, the relation of the impurity contents at the crystallization interface between the t and $t+1$ moments can be expressed by Langmuir-Knudsen equation as follows:

$$c_i(t+1)=\frac{j_i^+-j_i^-}{j_{\mathrm{Mg}}^+-j_{\mathrm{Mg}}^-}=\frac{j_i^+-\dfrac{c_i(t)P_i^o\sqrt{M_i}}{\sqrt{2\pi RT}}}{j_{\mathrm{Mg}}^+-\dfrac{P_{\mathrm{Mg}}^o\sqrt{M_{\mathrm{Mg}}}}{\sqrt{2\pi RT}}}=\frac{j_i^+-h_ic_i(t)\dfrac{P_i^o}{\sqrt{T}}}{j_{\mathrm{Mg}}^+-h_{\mathrm{Mg}}\dfrac{P_{\mathrm{Mg}}^o}{\sqrt{T}}}\#\# \tag{A.1}$$

where, the corner symbols i and Mg refer to the impurity i and Mg, respectively; j^+ is the condensation flux and irrelevant to the crystallization process, can be seen as a constant; j^- is the evaporation flux; $c_i(t)$ designates the impurity concentration at the t moment; M is the molar mass; h is the constant term in the Langmuir-Knudsen equation; T is the primary crystallization temperature.

When the crystallization process reaches a steady state, the impurity concentration will not vary with time. Then, $c_i(t+1)$ in Eq. (A.1) can be replaced by $c_i(t)$, transforming Eq. (A.1) into Eq. (A.2).

$$c_i(t)=\frac{j_i^+-h_ic_i(t)\dfrac{P_i^o}{\sqrt{T}}}{j_{\mathrm{Mg}}^+-h_{\mathrm{Mg}}\dfrac{P_{\mathrm{Mg}}^o}{\sqrt{T}}}\# \tag{A.2}$$

Solving for $c_i(t)$ in Eq. (A.2) yields:

$$c_i(t)=\frac{j_i^+}{j_{\mathrm{Mg}}^+-h_{\mathrm{Mg}}\dfrac{P_{\mathrm{Mg}}^o}{\sqrt{T}}+h_i\dfrac{P_i^o}{\sqrt{T}}}\# \tag{A.3}$$

It is clear that $c_i(t)$ is a function of temperature(T). Taking the derivative of $c_i(t)$ with respect to T, we obtain:

$$\frac{d(c_i)}{dT}=\frac{j_i^+}{\left(j_{\mathrm{Mg}}^+-h_{\mathrm{Mg}}\frac{P_{\mathrm{Mg}}^o}{\sqrt{T}}+h_i\frac{P_i^o}{\sqrt{T}}\right)^2}\times\frac{h_{\mathrm{Mg}}}{2\sqrt{T}}\times\left[\sqrt{\frac{M_i}{M_{\mathrm{Mg}}}}\times\left(\frac{P_i{}^o}{T}-2\frac{dP_i{}^o}{dT}\right)-\left(\frac{P_{\mathrm{Mg}}{}^o}{T}-2\frac{dP_{\mathrm{Mg}}{}^o}{dT}\right)\right]\# \tag{A.4}$$

The sign of $\mathrm{d}(c_i)/\mathrm{d}T$ only depends on the terms within the square brackets in eq. (A.4). Then, we can extract the terms and graph these as a curve depicted in Fig. 1(d).

Appendix B. Activity coefficient of impurities in Al melt

The formula (1) in the main text describes how the activity coefficient of solute element X in an Al–X binary solution determines its equilibrium partial pressure. As shown in Fig. B1, Ni, Fe, Ti, Ca, Cu, and Mn form negative-deviation solutions with Al, with their activity coefficients remaining below 0.01 within the solubility limit. In contrast, Pb and Zn exhibit activity coefficients close to unity in the Al binary solution, with the activity coefficient of Pb always remaining above one

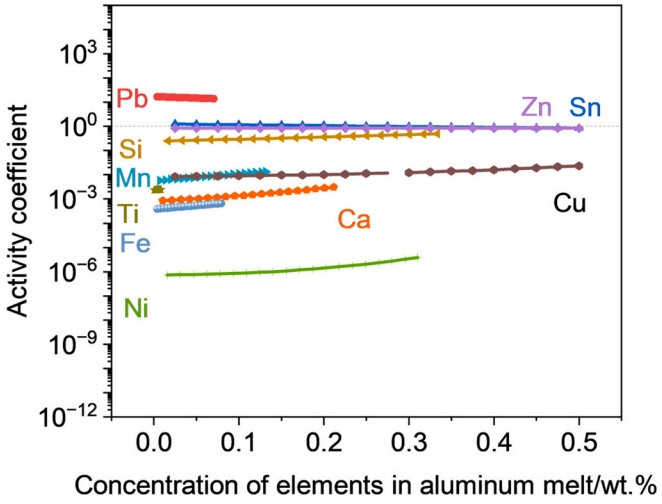


Fig. B1. Activity coefficient of impurities in Al melt at 850 °C.

Appendix C. Impurity deposits on Ti mesh

Fig. C1 shows the morphology and composition of impurities deposited on the Ti mesh after crude Mg evaporation. In addition to the Fe, Ca, and Cl impurities observed in Fig. 3(c), Al and Si were also detected. Mg deposits were relatively concentrated (Fig. C1(c)), whereas Al, Si, and Ca were uniformly distributed across the mesh (Fig. C1(e))

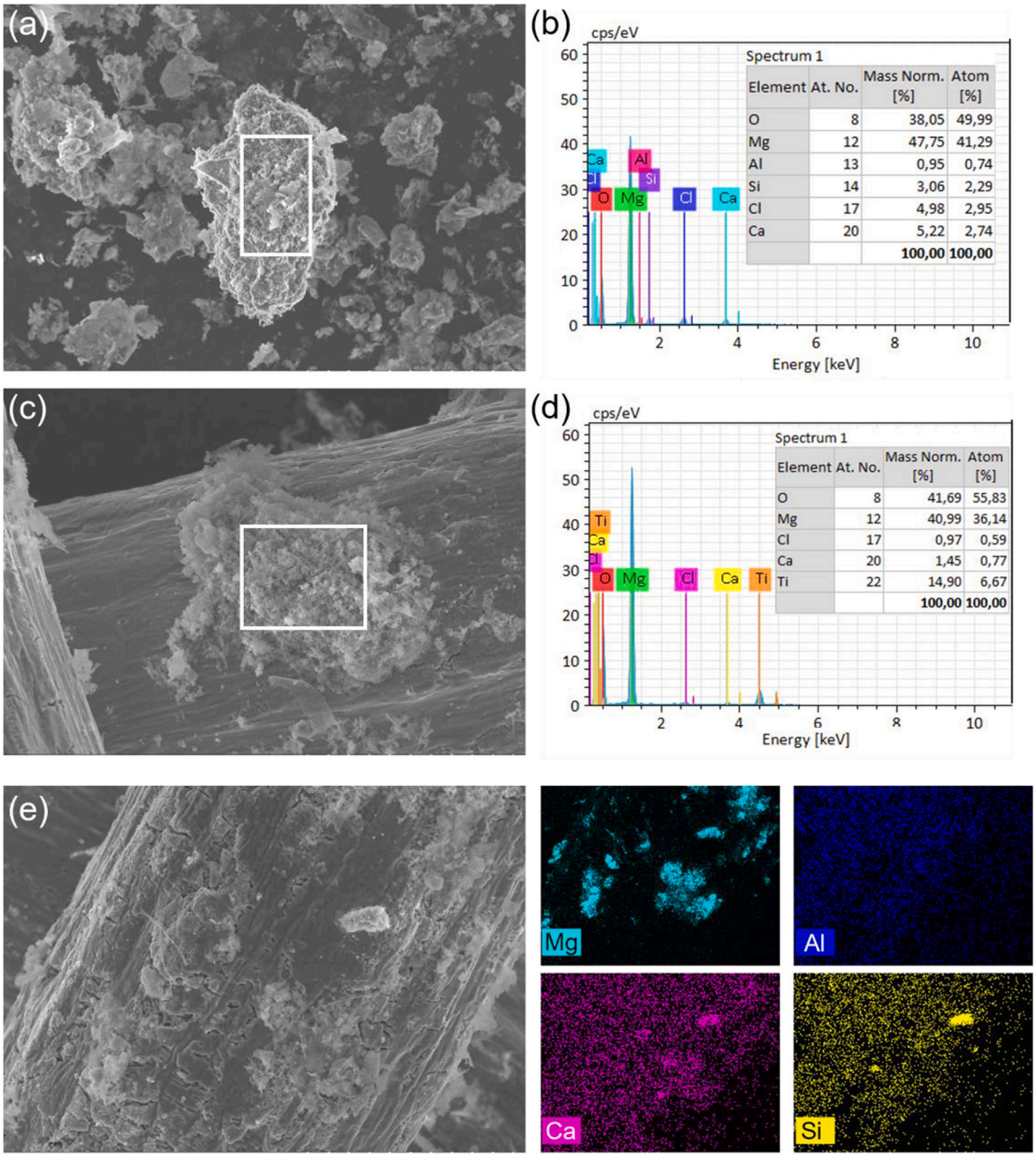


Fig. C1. The morphologies and compositions of the impurity deposits on the Ti mesh after the direct evaporation of crude Mg.

As shown in Fig. C2, the morphology and composition of impurities deposited on the Ti mesh after crude Mg evaporation with the concentric tubes structure included Al, Si, Ca, and Cl. Together with the Fe impurity in Fig. 3f, it can be concluded that introducing the concentric tubes did not change the impurity species in crude Mg.

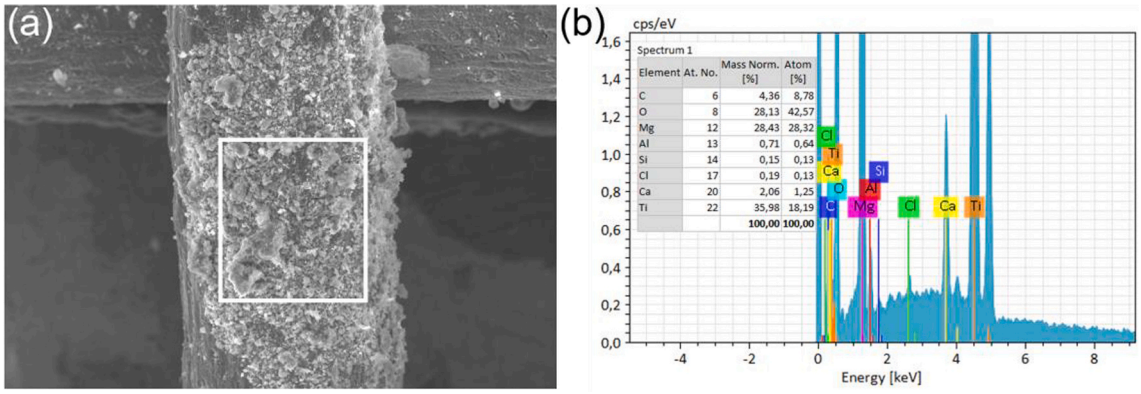


Fig. C2. The morphologies and compositions of the impurity deposits on the Ti mesh after the evaporation of crude Mg with the concentric tubes.

Data availability

The data that support the findings of this study are available from the corresponding authors on request.

References

[1] S.K. Woo, B.-C. Suh, H.S. Kim, C.D. Yim, Effect of Al addition on corrosion behavior of high-purity Mg in terms of processing history, J. Magnes. Alloys 11 (2023) 851–868, https://doi.org/10.1016/j.jma.2022.12.005.

[2] M. Esmaily, J.E. Svensson, S. Fajardo, N. Birbilis, G.S. Frankel, S. Virtanen, R. Arrabal, S. Thomas, L.G. Johansson, Fundamentals and advances in magnesium alloy corrosion, Prog. Mater. Sci. 89 (2017) 92–193, https://doi.org/10.1016/j.pmatsci.2017.04.011.

[3] D. Höche, C. Blawert, S.V. Lamaka, N. Scharnagl, C. Mendis, M.L. Zheludkevich, The effect of iron re-deposition on the corrosion of impurity-containing magnesium, Phys. Chem. Chem. Phys. 18 (2015) 1279–1291, https://doi.org/10.1039/C5CP05577F.

[4] J. Lee, G. Han, Y. Kim, J. Byun, J. Jang, H.-K. Seok, S. Yang, Effects of impurities on the biodegradation behavior of pure magnesium, Met. Mater. Int. 15 (2009) 955–961, https://doi.org/10.1007/s12540-009-0955-1.

[5] D. Mei, Y. Li, X. Ma, L. Wang, S. Zhu, S. Guan, The inhibition effect of etidronate on degradation behavior of Mg–Zn–Y-Nd-Zr alloy, Smart Mater. Manuf. 2 (2024) 100020, https://doi.org/10.1016/j.smmf.2023.100020.

[6] L. Yang, G. Liu, L. Ma, E. Zhang, X. Zhou, G. Thompson, Effect of iron content on the corrosion of pure magnesium: critical factor for iron tolerance limit, Corros. Sci. 139 (2018) 421–429, https://doi.org/10.1016/j.corsci.2018.04.024.

[7] B. Yang, R. Zheng, G. Wu, Z.M. Chang, Z.W. Shan, Minimizing pest aluminum in magnesium for the production of high-purity titanium, J. Magnes. Alloys 11 (2023) 4189–4196, https://doi.org/10.1016/j.jma.2022.05.016.

[8] B. Yang, B.Y. Liu, H. Yang, Z.W. Shan, A brief analysis of the importance of high-purity raw materials: the case of magnesium, Mater. China 39 (2020) 576–584.

[9] N. Xiong, S. Friedrich, S.R. Mohamed, I. Kirillov, X. Ye, Y. Tian, B. Friedrich, The separation behavior of impurities in the purification of high-purity magnesium via vacuum distillation, J. Sustain. Metall. 8 (2022) 1561–1572, https://doi.org/10.1007/s40831-022-00583-z.

[10] Jafar Safarian, T.A. Engh, Vacuum evaporation of pure metals, Metall. Mater. Trans. A 44 (2013) 747–753, https://doi.org/10.1007/s11661-012-1464-2.

[11] D. Liang, L. Wang, Y. Tian, B. Yang, B. Xu, W. Zhao, T. Ma, Preparation of high purity magnesium by vacuum gasification-directional condensation technology, Sep. Purif. Technol. 327 (2023) 124878, https://doi.org/10.1016/j.seppur.2023.124878.

[12] A.G. Guézennec, J.C. Huber, F. Patisson, Ph. Sessiecq, J.P. Birat, D. Ablitzer, Dust formation by bubble-burst phenomenon at the surface of a liquid steel bath, ISIJ Int. 44 (2004) 1328–1333, https://doi.org/10.2355/isijinternational.44.1328.

[13] N. Reinke, A. Voßnacke, W. Schütz, M.K. Koch, H. Unger, Aerosol generation by bubble collapse at ocean surfaces, Water Air Soil Pollut. Focus 1 (2001) 333–340, https://doi.org/10.1023/A:1013188029495.

[14] N. Singh, M. Kroells, C. Li, E. Ching, M. Ihme, C.J. Hogan, T.E. Schwartzentruber, General drag coefficient for flow over spherical particles, AIAA J. 60 (2022) 587–597, https://doi.org/10.2514/1.J060648.

[15] R. Li, L. Wang, B. Yang, B. Xu, D. Liang, F. Wang, Y. Tian, Magnesium alloy scrap vacuum gasification—directional condensation to purify magnesium, Metals 13 (2023) 675, https://doi.org/10.3390/met13040675.

[16] D. Liang, Y. Tian, B. Yang, N. Xiong, F. Wang, B. Xu, One-step preparation of high purity magnesium by vacuum distillation technology, Vacuum 192 (2021) 110464, https://doi.org/10.1016/j.vacuum.2021.110464.

[17] Y. Tian, X. Zhang, T. Qu, F. Lyu, H. Du, L. Shi, B. Yang, Y. Dai, Technical research on vacuum distillation to purify magnesium to 99.99% purity, Mater Res Express 8 (2021), https://doi.org/10.1088/2053-1591/abdf12.

[18] D. Liang, L. Wang, T. Ma, R. Yu, Y. Tian, B. Xu, B. Yang, Deep removal impurities in the process of preparing high-purity magnesium by vacuum gasification, J. Magnes. Alloys (2024), https://doi.org/10.1016/j.jma.2024.11.010.

[19] Z.W. Shan, B. Yang, B.Y. Liu, A. Wang, L.Y. Mao, J. Li, F. Liu, Z.M. Chang, A Method and Device for Vapor-Phase Magnesium Purification Based on Nickel-Based Filter Material, CN110835695A, 2020.

[20] Z.W. Shan, B. Yang, P.F. Wang, B.Y. Liu, L.Y. Mao, A. Wang, The Application of Pure iron Filter Material in Vapor-Phase Magnesium Purification and the Production System Incorporating it, CN110791665A, 2020.

[21] Z.W. Shan, Y.X. Hou, B. Yang, B.Y. Liu, P.C. Zhang, A. Wang, L.Y. Mao, A Method and Device for Vapor-Phase Magnesium Purification Based on Elemental Silicon Filter Material, CN110724833A, 2020.

[22] R.A. Swalin, A. Martin, Solute diffusion in nickel-base substitutional solid solutions, JOM 8 (1956) 567–571, https://doi.org/10.1007/BF03377730.

[23] J. Kučera, K. Stránský, Diffusion in iron, iron solid solutions and steels, Mater. Sci. Eng. 52 (1982) 1–38, https://doi.org/10.1016/0025-5416(82)90067-2.

[24] S. Gao, K. Jiao, J. Zhang, Review of viscosity prediction models of liquid pure metals and alloys, Philos. Mag. 99 (2019) 853–868, https://doi.org/10.1080/14786435.2018.1562281.

[25] N.B. Vargaftik, V.S. Yargin, Alkali-metal liquid and vapor thermophysical properties, J. Eng. Phys. 54 (1988) 109–118, https://doi.org/10.1007/BF00870239.

[26] Changjiang Nonferrous Metals Trading Market, Nonferrous Metal Prices. https://www.ccmn.cn/, 2025 (accessed January 27, 2025).

[27] G. Revel, J.-L. Pastol, J.-C. Rouchaud, R. Fromageau, Purification of magnesium by vacuum distillation, Metall. Trans. B 9 (1978) 665–672, https://doi.org/10.1007/BF03257216.

[28] J.L. Murray, The Mg−Ti (magnesium-titanium) system, Bull. Alloy Phase Diagr. 7 (1986) 245–248, https://doi.org/10.1007/BF02868999.

[29] B.R. Munson, T.H. Okiishi, W.W. Huebsch, A.P. Rothmayer, Fluid Mechanics, Wiley, 2013. https://dlib.scu.ac.ir/bitstream/Hannan/355519/2/97811183 18676.pdf (accessed September 2, 2025).

[30] I. Ohnuma, Y. Fujita, H. Mitsui, K. Ishikawa, R. Kainuma, K. Ishida, Phase equilibria in the Ti–Al binary system, Acta Mater. 48 (2000) 3113–3123, https://doi.org/10.1016/S1359-6454(00)00118-X.

[31] Y.C. Wang, Y. Tian, T. Qu, B. Yang, Y.N. Dai, Y.P. Sun, Purification of magnesium by vacuum distillation and its analysis, Mater. Sci. Forum 788 (2014) 52–57, https://doi.org/10.4028/www.scientific.net/MSF.788.52.

[32] S.L. Xia, Preliminary investigation on the preparation methods and sublimation purification mechanism of high-purity magnesium, Light Met. 40–45 (1986).

[33] H.L. Li, R. Hu, W.T. Qu, J.K. Yu, High purification of magnesium and magnesium alloys, Spec. Cast. Nonferrous Alloys (2001) 87–89.

[34] Q. Li, Z.F. Hu, Z.Q. Li, H.L. Jiang, Y.X. Yin, J.T. Jia, Producing high-purity magnesium by vacuum distillation, Non-Ferr. Metall. Eng. 4 (2014) 21–23.

[35] Y.C. Wang, Research on Preparation of High-Purity Magnesium by Vacuum Distillation, Master thesis, Kunming University of Science and Technology, 2015, https://kns.cnki.net/kcms2/article (accessed January 15, 2025).

[36] Y.J. Wu, Producing the Ultra High Purity Magnesium by Vacuum Distillation Method, Master thesis, University of Science and Technology Beijing, 2007.

[37] V.L. Matkovic, V.D. Manojlovic, M.D. Sokic, B.R. Markovic, Z.P. Gulisija, Z. J. Kamberovic, Optimal conditions of vacuum distillation process for obtaining the high grade pure magnesium, Tehnika 69 (2014) 58–62.

[38] I.I. Papirov, A.I. Kravchenko, A.V. Shiyan, A.I. Mazin, Removal of low-volatile impurities from magnesium by sublimation, Inorg. Mater. 50 (2014) 452–454, https://doi.org/10.1134/S0020168514050148.

[39] A.I. Kravchenko, Influence of the degree of distillation on the effective separation factor in some metallic host-impurity systems, Inorg. Mater. 51 (2015) 106–107, https://doi.org/10.1134/S0020168515010094.
[40] Y.P. Bobrov, V.D. Virich, P.N. V'yugov, N.P. V'yugov, S.D. Lavrinenko, M. M. Pylypenko, I.G. Tantsyura, High purity magnesium obtaining, Probl. At. Sci. Technol. (2018) 50–53.
[41] Y. Tian, Theoretical and Experimental Study on the Preparation of High-Purity Magnesium and Impurity Separation, Master thesis, Kunming University of Science and Technology, 2022, https://doi.org/10.27200/d.cnki.gkmlu.2021.000836.